Computational Materials Science 198 (2021) 110673

Contents lists available at ScienceDirect

Computational Materials Science

journal homepage: www.elsevier.com/locate/commatsci

Letter

Spatial and temporal heterogeneity of Kohlrausch–Williams–Watts stress relaxations in metallic glasses

Akio Ishii

Department of Mechanical Science and Bioengineering, Osaka University, 1-3 Machikaneyama, Toyonaka, Osaka 560-8531, Japan

ARTICLE INFO

Keywords:
Kohlrausch–Williams–Watts (KWW) relaxation
Metallic glass
Molecular dynamics (MD)

ABSTRACT

We perform a molecular dynamics (MD) stress relaxation simulation for $Zr_{50}Cu_{40}Al_{10}$ metallic glass to confirm that the time dependency of stress relaxation conforms with the Kohlrausch–Williams–Watts (KWW) equation, and to derive the temperature dependency of the Kohlrausch exponent β^{KWW}. We also calculate local plastic deformation based on atomic strain, then discuss the morphology of relaxation and calculate the probability density of stress relaxation with respect to the characteristic time of relaxation from the number of deformed atoms. Afterward, we derive the time dependency of stress relaxation as a mode-averaged decay function, which expresses spatial and temporal heterogeneity. Both the results of simulation and calculation reproduce the KWW relaxation form and are in good agreement, confirming the spatially and temporally heterogeneous nature of KWW relaxation. The heterogeneity of the stress relaxation of metallic glass is determined by local stress changes caused by microscopic local plastic deformation.

Kohlrausch–Williams–Watts (KWW) relaxation [1–3] is a well-known relaxation process that is often observed in glass and polymer materials. Its decay function is defined as follows:

$$\phi^{KWW}(t) = \phi_0^{KWW}\exp\left(-\left(\frac{t}{\tau^{KWW}}\right)^{\beta^{KWW}}\right). \quad (1)$$

ϕ_0^{KWW} is a prefactor, and τ^{KWW} is the characteristic time of the KWW relaxation. β^{KWW} is called the Kohlrausch exponent and usually ranges from 0 to 1 (stretched exponential). Reported values include $\beta^{KWW} \approx 0.35$ for spin glass, and $\beta^{KWW} \approx 0.6$ for glassy materials and polymers [4–7]. Because the decay function form (1) of KWW relaxation is empirical, its physical origin is investigated both experimentally and theoretically to understand the mechanism of KWW relaxation [5,8–10]. In particular, for metallic glass, which is a promising structural material, understanding the mechanism of KWW relaxation, which is always observed as β relaxation at temperatures lower than the glass transition temperature T_g [11], is important because the mechanical properties of metallic glass are always affected by relaxation and rejuvenation processes [12,13].

Recently, researchers derived the physical origin of KWW relaxation in terms of the spatial and temporal heterogeneity of relaxation [14], where heterogeneity increases as β^{KWW} decreases. For metallic glass, both experimental and theoretical evidence of the spatial heterogeneity of β relaxation has been reported. For β relaxation, the morphology of the relaxation process is spatially heterogeneous, and β^{KWW} decreases as the temperature decreases. By contrast, for homogeneous α relaxation, $\beta^{KWW} \approx 1$ at temperatures of approximately T_g [5,14–17]. Although the aforementioned efforts provide a clearer vision of the physical background of KWW relaxation, we believe that the detailed analysis is still insufficient. Conventionally, the decay function of a single relaxation is expressed in exponential form,

$$\phi(t) = \phi_0\exp\left(-\frac{t}{\tau}\right). \quad (2)$$

ϕ_0 is a prefactor, and τ is the characteristic time of relaxation. When spatial or temporal heterogeneity exists in relaxation, multiple relaxation modes with different characteristic times τ are expected. Thus, the decay function is defined based on the integral of the decay function of each relaxation mode, which is based on the probability density $g(\tau)$ ($\int_0^\infty g(\tau)d\tau = 1$) of that relaxation mode:

$$\phi^{mod}(t) = \phi_0\int_0^\infty g(\tau)\exp\left(-\frac{t}{\tau}\right)d\tau = \phi_0\left\langle\exp\left(-\frac{t}{\tau}\right)\right\rangle. \quad (3)$$

Although Ranko suggests that this heterogeneity determines the nature of KWW relaxation, i.e., $\phi^{KWW} \approx \phi^{mod}$ [14], to our knowledge, few studies have directly related the KWW Eq. (1) to the aforementioned

E-mail address: ishii@me.es.osaka-u.ac.jp.

https://doi.org/10.1016/j.commatsci.2021.110673
Received 17 May 2021; Received in revised form 13 June 2021; Accepted 16 June 2021
Available online 2 July 2021

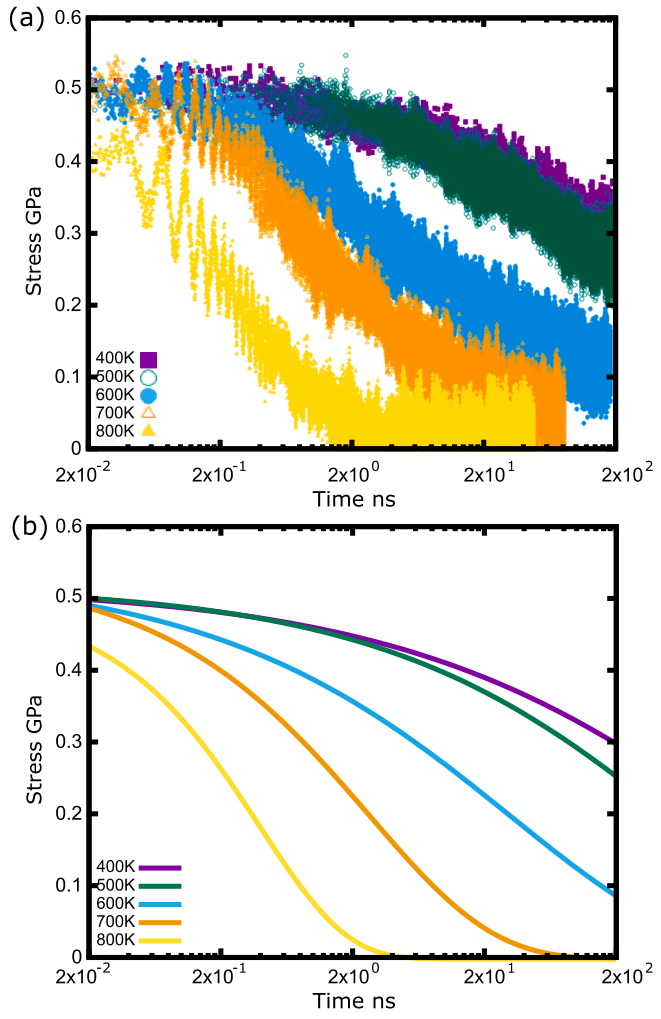

Fig. 1. $\sigma(t)$ plot of MD stress relaxation simulation, (a) raw data of MD simulation, (b) fitting curves of raw data using KWW stress relaxation Eq. (4).

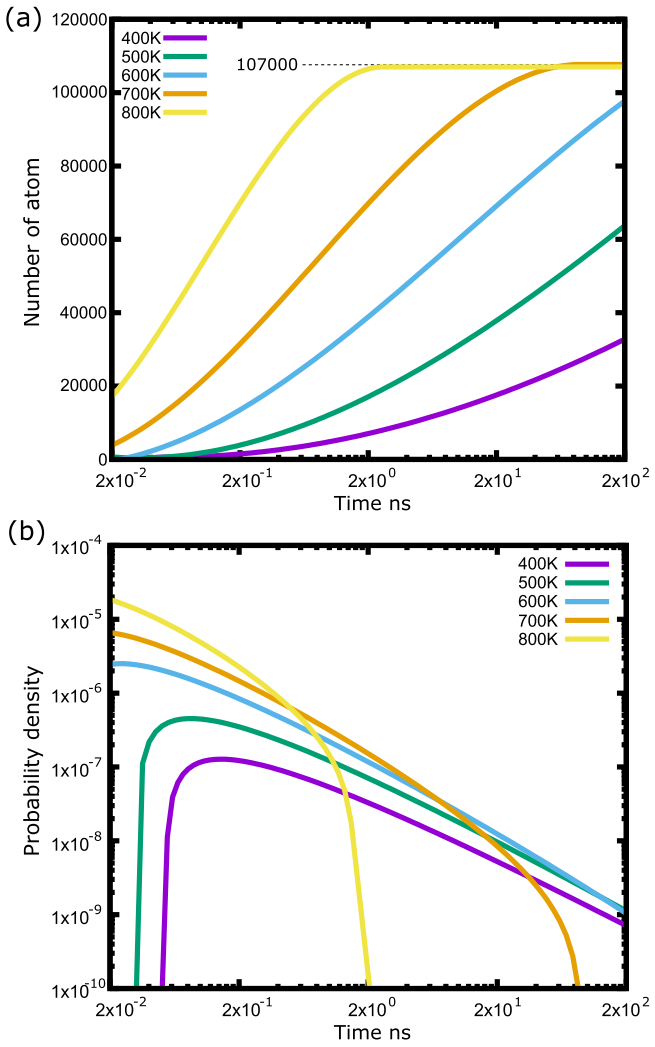

Fig. 2. Calculated (a) $N(\tau)$ and (b) $g_{sr}(\tau)$ curves at each temperature.

Table 1
KWW β^{KWW} values calculated via fitting of (a) direct MD data of $\sigma(t)$ and (b) mode-averaged $\sigma^{mod}(t)$ using KWW stress relaxation Eq. (4).

Temperature K	(a)	(b)
400	0.29	0.27
500	0.33	0.30
600	0.32	0.36
700	0.46	0.45
800	0.66	0.67

mode-average decay function (3). Additionally, for metallic glass, some studies also reported $\beta^{KWW} > 1$ (compressive exponential) KWW relaxation [9,18,19]. In this case, heterogeneity is not suitable for explaining KWW relaxation.

In this study, to determine the stress relaxation process of amorphous-structured metallic glass, we investigate the relationship between KWW relaxation and the spatial and temporal heterogeneity of relaxation. We perform molecular dynamics (MD) stress relaxation simulations [5,7] for $Zr_{50}Cu_{40}Al_{10}$ metallic glass to confirm that the time dependency of stress relaxation conforms to the KWW relaxation Eq. (1), and to derive the temperature dependency of β^{KWW}. On the other hand, parallel to the simulation, we calculate local plastic deformation based on atomic strain [20], then discuss the morphology of relaxation and calculate the probability density $g_{sr}(\tau)$ of stress relaxation from the number of deformed atoms. Using the calculated $g_{sr}(\tau)$, we derive the mode-averaged decay function of stress relaxation and compare it with the direct result of MD simulation.

First, let us explain our MD simulation of stress relaxation. The $Zr_{50}Cu_{40}Al_{10}$ atomic model, which consists of 125000 atoms, is prepared using Shen et al. embedded atom method (EAM) potential [21]. Meanwhile, LAMMPS [22] code is used for the simulation itself. The time step of MD simulation is set to 2 fs. We arrange the atoms randomly in the MD simulation box and melt the structure by keeping the model at 2000 K and zero stress for 1 ns under the NPT ensemble. Subsequently, a metallic glass model with a size of $13 \times 13 \times 13$ nm is created via quenching of the melted model at a constant cooling rate of 4.0×10^{11} K/s from 2000 K to 0 K. Based on discontinuity in the volume vs. temperature curve, we confirm that the glass transition temperature T_g is approximately 900 K. For the temperatures under T_g, i.e., 400 K, 500 K, 600 K, 700 K, and 800 K, we apply 0.5 GPa uniaxial compressive stress for 0.4 ns to our metallic glass model under the NPT ensemble. We then implement 200 ns, 100 ns, and 50 ns NVT ensemble simulations as stress relaxation simulations for temperatures 400 K to 600 K, 700 K, and 800 K. We confirm that the 0.5 GPa compressive stress is much lower than the yield stress of the metallic glass model at 300 K, which is 2.5 GPa.

During the stress relaxation simulation, we observe that compressive stress decreases as time elapses, and eventually, we confirm that the stress relaxation follows Eq. (1), which is the KWW relaxation form. Furthermore, we evaluate the temperature dependency of the Kohlrausch exponent parameter β^{KWW} by fitting the data to the following

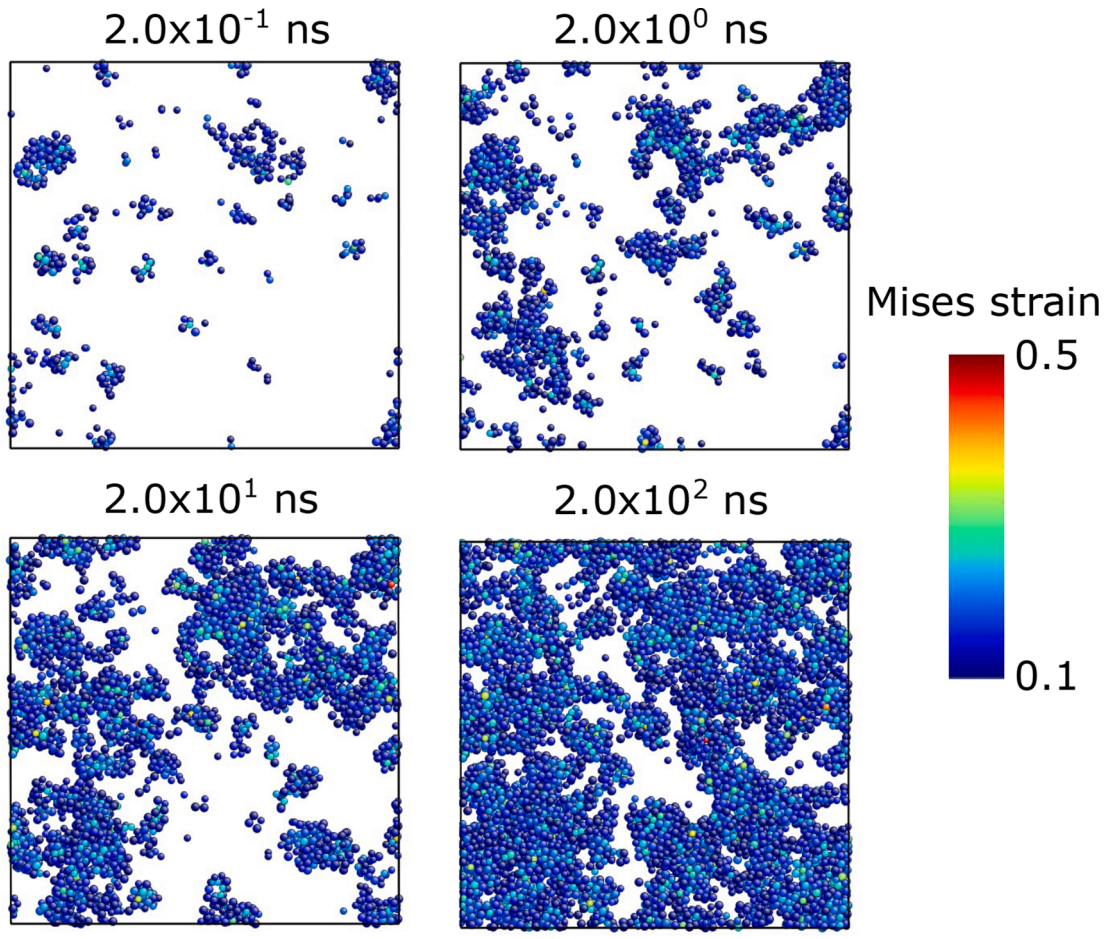

Fig. 3. Atomic von Mises strain distribution [34] at certain plane in metallic glass model during MD stress relaxation simulation at 500 K. Atomic strain coloring is prepared using AtomEye [34].

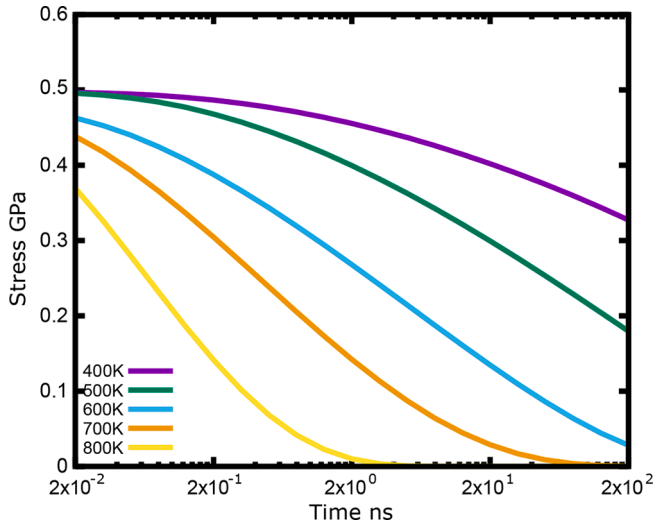

Fig. 4. Calculated $\sigma^{\mathrm{mod}}(t)$ curves at each temperature. σ_0 is set to 0.5 GPa.

KWW stress relaxation form:

$$\sigma(t) = \sigma_0 \exp\left(- \left(\frac{t}{\tau^{\mathrm{KWW}}} \right)^{\beta^{\mathrm{KWW}}} \right). \tag{4}$$

The initial stress σ_0 (approximately 0.5 GPa), Kohlrausch exponent β^{KWW}, and the characteristic time of KWW relaxation τ^{KWW} are fitting parameters. We show the raw data of the time vs. stress plot of the MD stress relaxation simulation in Fig. 1(a) and fitting curves in Fig. 1(b). The temperature dependency of the Kohlrausch exponent β^{KWW} of the MD simulation is shown in Table 1(a). We confirm that the standard errors of all fitting curves are lower than 8%. According to Table 1(a), the β^{KWW} values are in the range from 0.3 to 0.7 and decrease as

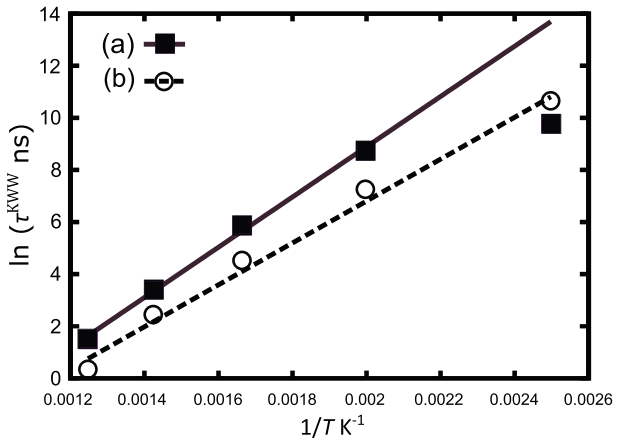

Fig. A.1. Inverse of temperature vs. log of KWW characteristic time τ^{KWW} of stress relaxation. τ^{KWW} is calculated via fitting of (a) MD data of $\sigma(t)$ and (b) mode-averaged $\sigma^{\mathrm{mod}}(t)$ using KWW stress relaxation equation (Eq. (4)).

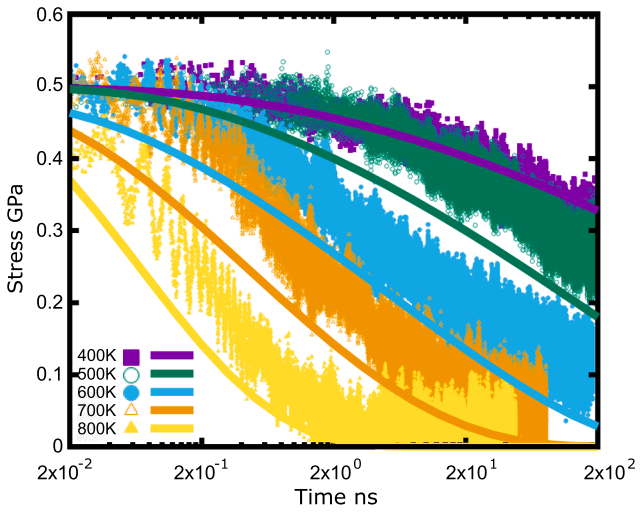

Fig. B.1. Calculated $\sigma^{\mathrm{mod}}(t)$ curves and the raw data of $\sigma(t)$ (plots) from MD stress relaxation simulation.

temperature decreases. This is consistent with a previous experimental result [5]. If the lower β^{KWW} value indicates that the relaxation is more spatially or temporally heterogeneous, our result indicates that heterogeneity becomes more prominent as the temperature decreases.

Afterward, we identify the local plastic deformation by calculating the atomic strain [20], and then discuss the morphology of relaxation and calculate the probability density $g_{\mathrm{sr}}(\tau)$ of stress relaxation from the number of deformed atoms. To the atomic structure of the MD stress relaxation simulation at a certain temperature and time, we first implement 0 K structural relaxation to remove thermal vibration effect on the atomic strain and to relax the atomic structure to its "plastic-deformed" local minima, and then calculate the atomic strain for each structural-relaxed atom based on a reference atomic structure, which is the atomic structure at time zero. Under the assumption that the characteristic time τ of stress relaxation is equivalent to the time of occurrence of local plastic deformation, we count the number of deformed atoms per 10,000 MD time steps and calculate continuous $N(\tau)$ curves via data fitting. The probability density $g_{\mathrm{sr}}(\tau)$ for stress relaxation is calculated as the derivative of $N(\tau)$:

$$g_{\mathrm{sr}}(\tau) = \frac{1}{N_{\max}}\frac{dN}{d\tau}, N_{\max} = \lim_{\tau\to\infty} N(\tau). \tag{5}$$

Deformed atoms are defined as atoms with von Mises atomic strains of 0.1 or higher. The von Mises atomic strain refers to the conventional plastic strain value of shear deformation of the shear transformation zone, which is an atomic cluster for local plastic deformation in metallic glass [23]. Using Eq. (3), we calculate the mode-averaged stress relaxation as

$$\sigma^{\mathrm{mod}}(t) = \sigma_0 \int_0^{\infty} g_{\mathrm{sr}}(\tau)\exp\left(-\frac{t}{\tau}\right)d\tau. \tag{6}$$

In contrast to a number of past studies, where spatial heterogeneity was investigated with respect to non-affine atomic displacement in MD simulations of metallic glass [7,9,24,25], in this study, we adopt atomic strain, which indicates affine atomic displacement, to directly determine local plastic deformation and change in stress. Conventionally, non-affine (or shuffling) and affine atomic displacement are cooperative, but sometimes, the cooperation is quite weak [26–28].

In Fig. 2, we show calculated (a) $N(\tau)$ and (b) $g_{\mathrm{sr}}(\tau)$ curves at each temperature. As the order of time increases, the number of deformed atoms increases, causing stress relaxation. At high temperatures, i.e., 700 and 800 K, $N(\tau)$ becomes a constant value ($\approx 107{,}000$) at a certain time, which is regarded as $N_{\max}$. The decrease in temperature flattens the $g_{\mathrm{sr}}(\tau)$ curve, indicating that stress relaxation becomes more heterogeneous. $g_{\mathrm{sr}}(\tau)$ distribution seems to transfer from a decaying mode to a flatter Gaussian like mode as temperature decreases, this is in good agreement with the estimation from energy barrier samplings by Han et al. [29]. Fig. 3 shows the atomic strain morphology change with respect to time on a certain plane of our metallic glass model (thickness is 1 nm) at 500 K. Clearly, we can observe that spatial and temporal heterogeneity exists. As time elapses, subsequent local plastic deformation occurs around the deformed region, increasing the number of deformed atoms $N(\tau)$, although the atomic strain in the already deformed region does not increase. This indicates that the spatially heterogeneous (or local) plastic deformation does not concentrate at a specific region but spreads to the entire metallic glass, reducing the macroscopic stress of metallic glass. Because heterogeneous plastic deformation is a thermally activated process, the characteristic time τ for the relaxation is associated with activation free energy ΔG of relaxation, which is dependent on local stress σ_{lc} [30,31], as follows:

$$\tau = \tau_0 \exp\left(\frac{\Delta G(\sigma_{\mathrm{lc}})}{k_{\mathrm{B}}T}\right). \tag{7}$$

τ_0 is a prefactor. In this sense, the subsequent plastic deformation in the deformed region is prevented by a reduction in local stress. On the other hand, the plastic deformation around the deformed region is activated by the increase in local stress caused by the local plastic strain in the deformed region [31,32]. Thus, the spatial or temporal heterogeneity is determined by local stress changes caused by microscopic local plastic deformation. Moreover, from atomic strain morphology, the temporal evolutions of atomic strain distribution seems to involve three processes: activation of plastic deformation events of individual shear transformation zone, cascade or cluster of plastic deformation events, and percolation of plastic deformation events, that agrees with the recent Cao et al. study, which reveals atomic strains activated on three levels of energy barrier hopping [33].

Finally, we show $\sigma^{\mathrm{mod}}(t)$ plot and β^{KWW} values calculated using $g_{\mathrm{sr}}(\tau)$ and Eq. (6) in Fig. 4 and Table 1(b), respectively. β^{KWW} values were calculated via fitting of mode-averaged $\sigma^{\mathrm{mod}}(t)$ using the KWW stress relaxation Eq. (4). These calculated values were compared with the direct result of the MD simulation, i.e., Fig. 1 and Table 1(a). Although little discrepancy exists between the characteristic time τ^{KWW} of the MD simulation result for $\sigma(t)$ and $\sigma^{\mathrm{mod}}(t)$ from the fitting curves, we believe both results generally have good agreement. Eventually, we successfully reproduced the KWW relaxation Eq. (4) from the mode-average decay function (3) for the stress relaxation of metallic glass. For the exact value of the discrepancy and the comparison between $\sigma(t)$ and $\sigma^{\mathrm{mod}}(t)$ curves, the reader can refer to our appendix figures, Figs. A.1 and B.1.

In summary, for the stress relaxation process of amorphous-structured metallic glass, we investigated the relationship between KWW relaxation and the spatial and temporal heterogeneity of relaxation. We perform a MD stress relaxation simulation for $Zr_{50}Cu_{40}Al_{10}$ metallic glass to confirm that the time dependency of stress relaxation conforms to the KWW relaxation form, and to derive the temperature dependency of the β^{KWW}. Meanwhile, parallel to the simulation, we identify the local plastic deformation by calculating the atomic strain, then discuss the morphology of relaxation and calculate the probability density $g_{\mathrm{sr}}(\tau)$ of stress relaxation from the number of deformed atoms. Using the calculated probability density $g_{\mathrm{sr}}(\tau)$, we derive the time dependency of stress relaxation as a mode-averaged decay function, which describes the spatial and time heterogeneity of relaxation, and compare it with the direct result of MD simulation. Both results reproduce the KWW relaxation form and are in good agreement, confirming the spatial and time heterogeneous nature of KWW relaxation. The heterogeneity of the stress relaxation of metallic glass is dependent on local stress changes caused by microscopic local plastic deformation. Additionally, in the appendix, we also provide the activation energy data of the KWW stress relaxation derived from the Arrhenius equation.

CRediT authorship contribution statement

Akio Ishii: Conceptualization, Methodology, Validation, Investigation, Writing - original draft, Writing - review & editing, Visualization, Funding acquisition.

Declaration of competing interest

The authors declare that they have no known competing financial interests or personal relationships that could have appeared to influence the work reported in this paper.

Acknowledgements

This study was partially supported by a Grant-in-Aid for Early Career Scientists 18K13658 and Grant-in-Aid for Scientific Research (C) 21K03771. MD simulations were partly carried out through the use of OCTOPUS large-scale computer systems at the Cybermedia Center, Osaka University.

Appendix A. Activation energy of KWW stress relaxation

We also calculated the temperature dependency of the characteristic time τ^{KWW} of KWW stress relaxation by fitting the MD data and mode-averaged $\sigma^{\mathrm{mod}}(t)$ using KWW stress relaxation (Eq. (4)), as shown in the log plots of $\tau^{\mathrm{KWW}}(1/T)$ in the Fig. A.1(a) and (b), respectively. Except for the result at 400 K, the log plot of τ^{KWW} generally has a linear relationship with the inverse of temperature. Based on the Arrhenius equation,

$$\tau^{\mathrm{KWW}} = \tau_0^{\mathrm{KWW}} \exp\left(\frac{\Delta G^{\mathrm{KWW}}}{k_{\mathrm{B}} T}\right). \tag{A.1}$$

The macroscopic activation energy of KWW stress relaxation is derived from the gradient of the log plot of τ^{KWW} with respect to the inverse of temperature. The estimated activation energies from the gradients of the log plots (except for 400 K) are 0.83(a) and 0.70(b) eV, which are consistent with previous experiment and simulation results 0.37–1.2 eV for β relaxation of Zr-based metallic glass [35,36,10]. The outlier at 400 K is due to insufficient stress data due to the limitation of the MD time scale, and accelerated MD simulation [27,37] will be conducted in the future to solve the time scale problem. Related to this, although the empirical Vogel–Fulcher–Tammann (VFT) law $\tau = \tau_0 \exp\left(\frac{DT_0}{(T-T_0)}\right)$ (D, T_0 is parameters) is often used to describe the temperature dependency of τ^{KWW} [14], we do not discuss it in this study because the τ^{KWW} data at low temperatures are not sufficient because of the limitation of the MD simulation time scale.

Appendix B. Figure including $\sigma^{\mathrm{mod}}(t)$ curves and $\sigma(t)$ plots

We provide a figure including both calculated $\sigma^{\mathrm{mod}}(t)$ stress relaxation curves (in Fig. 4) and the raw data of $\sigma(t)$ from MD stress relaxation simulation (in Fig. 1(a)) as Fig. B.1. The reader can refer this figure for the comparison between calculated $\sigma^{\mathrm{mod}}(t)$ curves and $\sigma(t)$ from direct MD stress relaxation simulation. As we mentioned in the main text, the difference between $\sigma^{\mathrm{mod}}(t)$ curve and $\sigma(t)$ plot is mainly caused by the discrepancy between the characteristic time τ^{KWW} of the MD simulation result for $\sigma(t)$ and $\sigma^{\mathrm{mod}}(t)$.

References

[1] R. Kohlrausch, Prog. Ann. Phys. 91 (1854) 179–214.
[2] G. Williams, D.C. Watts, Trans. Faraday Soc. 66 (1970) 80–85.
[3] G. Williams, D.C. Watts, S.B. Dev, A.M. North, Trans. Faraday Soc. 67 (1971) 1323–1336.
[4] J.C. Phillips, Rep. Prog. Phys. 59 (1996) 1133–1207.
[5] Z. Wang, B.A. Sun, H.Y. Bai, W.H. Wang, Nature Comm. 5 (2014) 5823.
[6] Y. Yu, M. Wang, D. Zhang, B. Wang, G. Sant, M. Bauchy, Phys. Rev. Lett. 115 (2015), 165901.
[7] J.C. Qiao, Y.J. Wang, L.Z. Zhao, L.H. Dai, D. Crespo, J.M. Pelletier, L.M. Keer, Y. Yao, Phys. Rev. B 94 (2016), 104203.
[8] Q. Wang, S. Zhang, Y. Yang, Y. Dong, C. Liu, J. Lu, Nature Comm. 6 (2015) 7876.
[9] Z.W. Wu, W. Kob, W.H. Wang, L. Xu, Nature Comm. 9 (2018) 5334.
[10] Y.B. Yang, Q. Yang, D. Wei, L.H. Dai, H.B. Yu, Y.J. Wang, Phys. Rev. B 102 (2020), 174103.
[11] H.B. Yu, W.H. Wang, H.Y. Bai, K. Samwer, Nat. Sci. Rev. 1 (2014) 429–461.
[12] M. Wakeda, J. Saida, J. Li, S. Ogata, Sci. Rep. 5 (2015) 10545.
[13] N. Miyazaki, M. Wakeda, Y.J. Wang, S. Ogata, N.P.J. Comput, Mater. 2 (2016) 16013.
[14] R. Richert, J. Phys. Condens. Matter 14 (2002) 201.
[15] F. Zhu, H.K. Nguyen, S.X. Song, D.P. Aji, A. Hirata, H. Wang, K. Nakajima, M. W. Chen, Nature Comm. 7 (2016) 11516.
[16] D.P. Wang, J.C. Qiao, C.T. Liu, Mater. Res. Lett. 7 (2019) 305–311.
[17] J. Qiao, Q. Wang, J. Pelletier, H. Kato, R. Casalini, D. Crespo, E. Pineda, Y. Yao, Y. Yang, Prog. Mater. Sci. 104 (2019) 250–329.
[18] B. Ruta, Y. Chushkin, G. Monaco, L. Cipelletti, E. Pineda, P. Bruna, V.M. Giordano, M. Gonzalez-Silveira, Phys. Rev. Lett. 109 (2012), 165701.
[19] B. Ruta, G. Baldi, G. Monaco, Y. Chushkin, J. Chem. Phys. 138 (2013), 054508.
[20] F. Shimizu, S. Ogata, J. Li, Mater. Trans. 48 (2007) 2923–2927.
[21] H.W. Sheng, M.J. Kramer, A. Cadien, T. Fujita, M.W. Chen, Phys. Rev. B 83 (2011), 134118.
[22] S. Plimpton, J. Comput. Phys. 117 (1995) 1–19.
[23] A.S. Argon, Acta Metall. 27 (1979) 47–58.
[24] M. Wakeda, J. Saida, Sci. Tech. Adv. Mater. 20 (2019) 632–642.
[25] B. Wang, L. Wang, B. Shang, X. Gao, Y. Yang, H. Bai, M. Pan, W. Wang, P. Guan, Acta Mater. 195 (2020) 611–620.
[26] A. Ishii, J. Li, S. Ogata, Inter. J. Plas. 82 (2016) 32–43.
[27] P. Cao, M.P. Short, S. Yip, Proc. Natl. Acad. Sci. U.S.A. 114 (2017) 13631–13636.
[28] A. Ishii, Comput. Mater. Sci. 183 (2020), 109907.
[29] D. Han, D. Wei, P.H. Cao, Y.J. Wang, L.H. Dai, Phys. Rev. B 101 (2020) 64205.
[30] T. Egami, Prog. Mater. Sci. 56 (2011) 637–653.
[31] P. Zhao, J. Li, Y. Wang, Inter. J. Plas. 40 (2013) 1–22.
[32] T. Mura, Micromechanics of Defects in Solids, Springer Science & Business Media, Heidelberg, Germany, 2013.
[33] P. Cao, M.P. Short, S. Yip, Proc. Natl. Acad. Sci. U.S.A. 116 (2019) 18790–18797.
[34] J. Li, Model. Simul. Mater. Sci. Eng. 11 (2003) 173–177.
[35] A. Dubach, F.H. Torre, J.F. Lffler, Phil. Mag. Lett. 87 (2007) 695–704.
[36] H.B. Yu, K. Samwer, Y. Wu, W.H. Wang, Phys. Rev. Lett. 109 (2012), 095508.
[37] A. Ishii, S. Ogata, H. Kimizuka, J. Li, Phys. Rev. B 85 (2012), 064303.